Supplemental Material

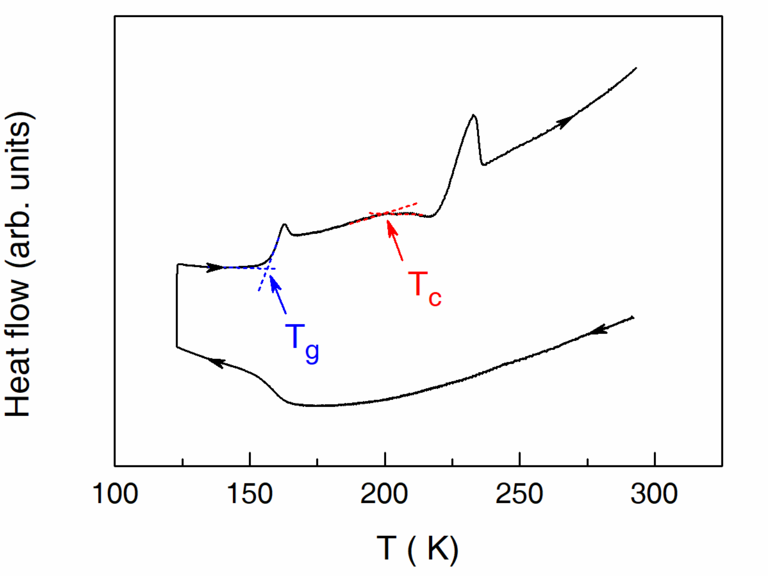

Fig. S1. DSC thermogram of aqueous glycerol solution with a mass fraction of water of X_w= 0.4. The cooling rate and heating rate are 3.0 and 0.7 K/min., respectively. T_g is defined as the onset temperature of glass-liquid transition, and T_c that of cold-crystallization of water.

Table S1. Ratio of the cold-crystallization temperature, T_c, to the glass transition temperature, T_g, for some metallic glasses, polymers, and aqueous solutions of electrolytes and small organic molecules.

	T_g	T_c	T_c/T_g
Glycerol·5H_2O[1]	155.68	185.63	1.19
Glycerol·4H_2O[1]	156.92	179.36	1.14
DMSO·5H_2O[1]	139.88	189.22	1.35
EG·4H_2O[1]	141.54	169.3	1.19
Butanetriol·5.3H_2O[1]	160.57	194.98	1.21
PEG300·14H_2O[1]	171.32	210.94	1.23
$Ca(NO_3)_2$·10H_2O[1]	172.4	206.21	1.19
$CrCl_3$·22H_2O[1]	150.66	206.26	1.36
$CrCl_3$·24H_2O[1]	149.07	174.23	1.16
$CrCl_3$·26H_2O[1]	149.53	168.08	1.12
$CaCl_2$·13H_2O[1]	154.44	204.92	1.32
$CaCl_2$·14H_2O[1]	152.83	202.95	1.32
$MnCl_2$·13H_2O[1]	154.01	203.49	1.32
$MnCl_2$·15H_2O[1]	150.13	190.81	1.27
$ZnCl_2$·12H_2O[1]	153.99	193.57	1.25
$MgCl_2$·18H_2O[1]	151.98	194.5	1.27
$FeCl_3$·22H_2O[1]	154.68	192.97	1.24
Sucrose.0.19H_2O[2]	333.15	398.15	1.19
Sucrose.0.28H_2O[2]	331.15	388.15	1.17
Sucrose.0.38H_2O[2]	323.15	373.15	1.15
Sucrose.0.61H_2O[2]	305.15	365.15	1.19
Sucrose[2]	347.15	403.15	1.16
Lactose[2]	381.15	458.15	1.20
Poly(L-lactic acid)[3]	328.35	377.35	1.14
PEEK[4]	419.0	446	1.06

Table SI. Continued.

	Tg	Tc	Tc/Tg
Isotactic polypropylene[5]	278.15	298.15	1.07
$Pd_{40}Ni_{10}Cu_{30}P_{20}$[6]	586	671	1.14
$La_{68}Ga_{10}Cu_{22}$[7]	375	424	1.13
$La_{68}Ga_{12}Cu_{20}$[7]	380	432	1.14
$La_{68}Ga_{14}Cu_{18}$[7]	391	435	1.11
$La_{70}Ga_{10}Cu_{20}$[7]	379	409	1.08
$La_{70}Ga_{12}Cu_{18}$[7]	382	438	1.15
$La_{70}Ga_{14}Cu_{16}$[7]	394	433	1.10
$La_{70}Ga_{16}Cu_{14}$[7]	401	452	1.13
$Y_{50}Ni_{20}Al_{30}$[8]	655	701	1.07
$Y_{55}Ni_{20}Al_{25}$[8]	639	669	1.05
$Y_{60}Ni_{20}Al_{20}$[8]	588	634	1.08
$La_{60}Ni_{20}Al_{20}$[8]	446	495	1.11
$Y_{60}Ni_{15}Al_{25}$[8]	588	664	1.13
$Y_{60}Co_{15}Al_{25}$[8]	648	678	1.05
$Y_{60}Fe_{15}Al_{25}$[8]	667	697	1.04
$La_{60}Ni_{15}Al_{25}$[9]	455	507	1.11
$La_{59}Ni_{15}Al_{25}Cu_{1}$[9]	454	508	1.12
$La_{58}Ni_{15}Al_{25}Cu_{2}$[9]	454	509	1.12
$La_{55}Ni_{15}Al_{25}Cu_{5}$[9]	457	538	1.18
$La_{52}Ni_{15}Al_{25}Cu_{8}$[9]	459	535	1.17
$La_{50}Ni_{15}Al_{25}Cu_{10}$[9]	464	537	1.16
$La_{60}Ni_{14}Al_{25}Cu_{1}$[9]	454	510	1.12
$La_{60}Ni_{13}Al_{25}Cu_{2}$[9]	449	499	1.11
$La_{60}Ni_{10}Al_{25}Cu_{5}$[9]	442	493	1.12
$La_{60}Ni_{15}Al_{24}Cu_{1}$[9]	449	519	1.16
$La_{60}Ni_{15}Al_{23}Cu_{2}$[9]	443	509	1.15

Table SI. Continued.

	Tg	Tc	Tc/Tg
$La_{60}Ni_{15}Al_{20}Cu_{5}$[9]	426	514	1.21
$La_{60}Ni_{15}Al_{17}Cu_{8}$[9]	416	485	1.17
$La_{60}Ni_{15}Al_{15}Cu_{10}$[9]	412	464	1.13
$La_{60}Ni_{15}Al_{10}Cu_{15}$[9]	401	434	1.08
$Tm_{39}Ce_{16}Co_{20}Al_{25}$[10]	608	663	1.09
$Tm_{39}Pr_{16}Co_{20}Al_{25}$[10]	611	666	1.09
$Tm_{39}Nd_{16}Co_{20}Al_{25}$[10]	621	701	1.13
$Tm_{39}Sm_{16}Co_{20}Al_{25}$[10]	631	693	1.10
$Tm_{39}Gd_{16}Co_{20}Al_{25}$[10]	646	717	1.11
$Tm_{39}Tb_{16}Co_{20}Al_{25}$[10]	650	711	1.09
$Tm_{39}Dy_{16}Co_{20}Al_{25}$[10]	657	701	1.07
$Tm_{39}Ho_{16}Co_{20}Al_{25}$[10]	666	719	1.08
$Tm_{39}Er_{16}Co_{20}Al_{25}$[10]	668	723	1.08
$Gd_{53}Al_{24}Co_{20}Zr_{3}$[10]	599	653	1.09
$Gd_{51}Al_{24}Co_{20}Zr_{4}Nb_{1}$[10]	598	653	1.09
$Dy_{36}Ho_{2}0Al_{24}Co_{20}$[10]	633	687	1.09
$Ho_{36}Dy_{20}Al_{24}Co_{20}$[10]	553	629	1.14
$Er_{50}Al_{24}Co_{20}Y_{6}$[10]	651	702	1.08
$Pd_{40}Ni_{22.5}Fe_{17.5}P_{20}$[10]	600	666	1.11
$Sr_{60}Mg_{18}Zn_{22}$[11]	331	374	1.13
$Sr_{60}Li_{11}Mg_{9}Zn_{20}$[11]	299	323	1.08
$Sr_{60}Li_{5}Mg_{15}Zn_{20}$[11]	315	336	1.07
$Sr_{60}Mg_{20}Zn_{15}Cu_{5}$[11]	335	374	1.12
$Sr_{40}Yb_{20}Mg_{20}Zn_{15}Cu_{5}$[11]	336	378	1.13
$Sr_{20}Yb_{20}Ca_{20}Mg_{20}Zn_{20}$[11]	353	389	1.10
$Sr_{20}Yb_{20}Ca_{20}Mg_{20}Zn_{10}Cu_{10}$[11]	351	391	1.11
$Ca_{60}Mg_{25}Cu_{15}$[12]	390	416	1.07

Table SI. Continued.

	Tg	Tc	Tc/Tg
$Ca_{55}Mg_{25}Cu_{20}$[12]	398	428	1.08
$Ca_{50}Mg_{25}Cu_{25}$[12]	400	439	1.10
$Ca_{45}Mg_{25}Cu_{30}$[12]	400	438	1.10
$Ca_{40}Mg_{25}Cu_{35}$[12]	399	436	1.09
$Ca_{35}Mg_{25}Cu_{40}$[12]	386	429	1.11
$Ca_{30}Mg_{25}Cu_{45}$[12]	387	430	1.11
$Ta_{42}Ni_{42}Co_{16}$[13]	998	1038	1.04
$Ta_{42}Ni_{40}Co_{18}$[13]	993	1032	1.03
$Ta_{42}Ni_{38}Co_{20}$[13]	1003	1038	1.03
$Ta_{42}Ni_{36}Co_{22}$[13]	1005	1035	1.03
$Ta_{46}Ni_{36}Co_{18}$[13]	991	1027	1.04
$Ta_{50}Ni_{32}Co_{18}$[13]	980	1015	1.04
$Yb_{70}Zn_{20}Mg_{10}$[14]	347	386	1.11
$Yb_{62.5}Zn_{20}Mg_{17.5}$[14]	367	398	1.08
$Yb_{64}Zn_{20}Mg_{15}Cu_{1}$[14]	357	402	1.13
$Yb_{65}Zn_{20}Mg_{10}Cu_{5}$[14]	384	419	1.09
$Yb_{62.5}Zn_{15}Mg_{17.5}Cu_{5}$[14]	381	401	1.05

1. The current work.
2. Saleki-Gerhardt, A. & Zografi, G., Non-isothermal and isothermal crystallization of sucrose from the amorphous state. *Pharm*. *Res*. **11**, 1166-1173 (1994).
3. Mano, J. F., Wang, Y. M., Viana, J. C., Denchev, A & Oliveira, M. J., Cold crystallization of PLLA studied by simultaneous SAXS and WAXS. *Macromol. Mater. Eng*. **289**, 910-915 (2004).
4. Cheng, S. Z. D., Cao, M. Y. & Wunderlich, B., Glass transition and melting behavior of poly(oxy-1,4-phenyleneoxy-1,4-phenylenecarbonyl-1,4-phenylene). *Macromolecules*. **19**, 1868-1876 (1986).

5. Schawe, J. E. K., Analysis of non-isothermal crystallization during cooling and reorganization during heating of isotactic polypropylene by fast scanning DSC. *Thermochim. Acta* **603**, 85-93 (2015).
6. Hu, X., Ng, S. C., Feng, Y. P. & Li, Y., Cooling-rate dependence of the density of $Pd_{40}Ni_{10}Cu_{30}P_{20}$ bulk metallic glass. *Phys. Rev. B* **64**, 172201 (2001).
7. Zhao, L. Z., Xue, R. J., Wang, W. H. & Bai, H. Y., LaGa-based bulk metallic glasses. *Chin. Phys. B* 26, 018106 (2017).
8. Luo, P., Lu, Z., Zhu, Z. G., Li, Y. Z., Bai, H. Y. & Wang, W. H., Prominent β-relaxation in yttrium based metallic glasses. *Appl. Phys. Lett.* **106**, 031907 (2015).
9. Zhu, Z. G., Li, Y. Z., Wang, Z., Gao, X. Q., Wen, P., Bai, H. Y., Ngai, K. L. & Wang, W. H., Compositional origin of unusual *β*-relaxation properties in La-Ni-Al metallic glasses. *J. Chem. Phys.***141**, 084506 (2014).
10. Huo, J. T., Zhao, D. Q., Bai, H. Y., Axinte, E. & Wang, W. H., Giant magnetocaloric effect in Tm-based bulk metallic glasses. *J. Non-Crystal. Solids* **359**, 1-4, 2013.
11. Zhao, K., Formation and properties of strontium-based bulk metallic glasses with ultralow glass transition temperature. *J. Mater. Res.*, **27**, 2539-2600 (2012).
12. Jiao, W., Zhao, D. Q., Ding, D. W., Bai, H. Y. & Wang, W. H., Effect of free electron concentration on glass-forming ability of Ca–Mg–Cu system. *J. Non-Crystal. Solids* **358**, 711-714 (2012).
13. Meng, D., Yi, J., Zhao, D. Q., Ding, D. W., Bai, H. Y., Pan, M. X. & Wang, W. H., Tantalum based bulk metallic glasses. *J. Non-Crystal. Solids* **357**,1787-1790 (2011).
14. Wang, J. Q., Wang, W. H. & Bai, H. Y., Soft ytterbium-based bulk metallic glasses with strong liquid characteristic by design. *Appl. Phys. Lett.* **94**, 041910 (2009).

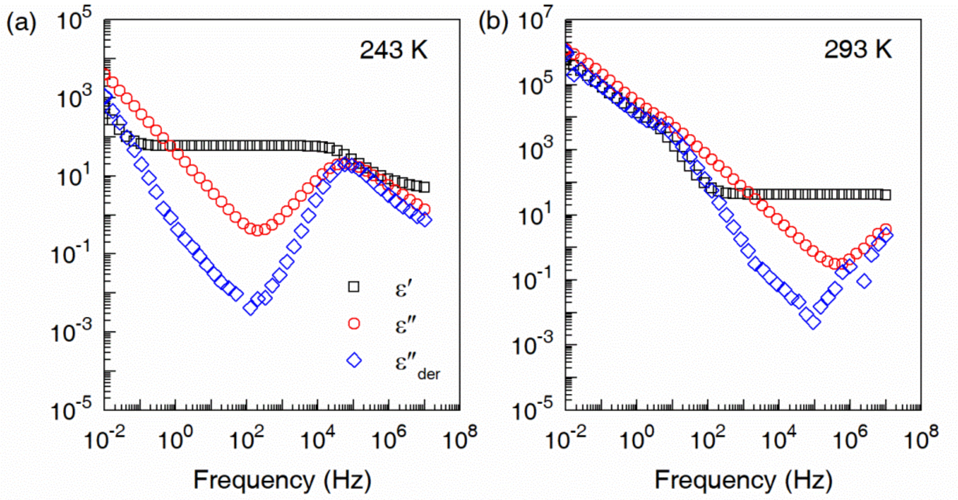

Fig. S2. Frequency dependence of ε' (square), ε'' (circle) and the derivative quantity $\varepsilon''_{der} = -\pi/2 \cdot \mathrm{d}\varepsilon'(\omega)/\mathrm{dln}(\omega)$ (diamond) for pure glycerol at (a) 243 K and (b) 293 K, respectively. Different from previous report, the low-frequency relaxation process in ε''_{der} around the frequency at which $\varepsilon' = \varepsilon''$ is not observable.

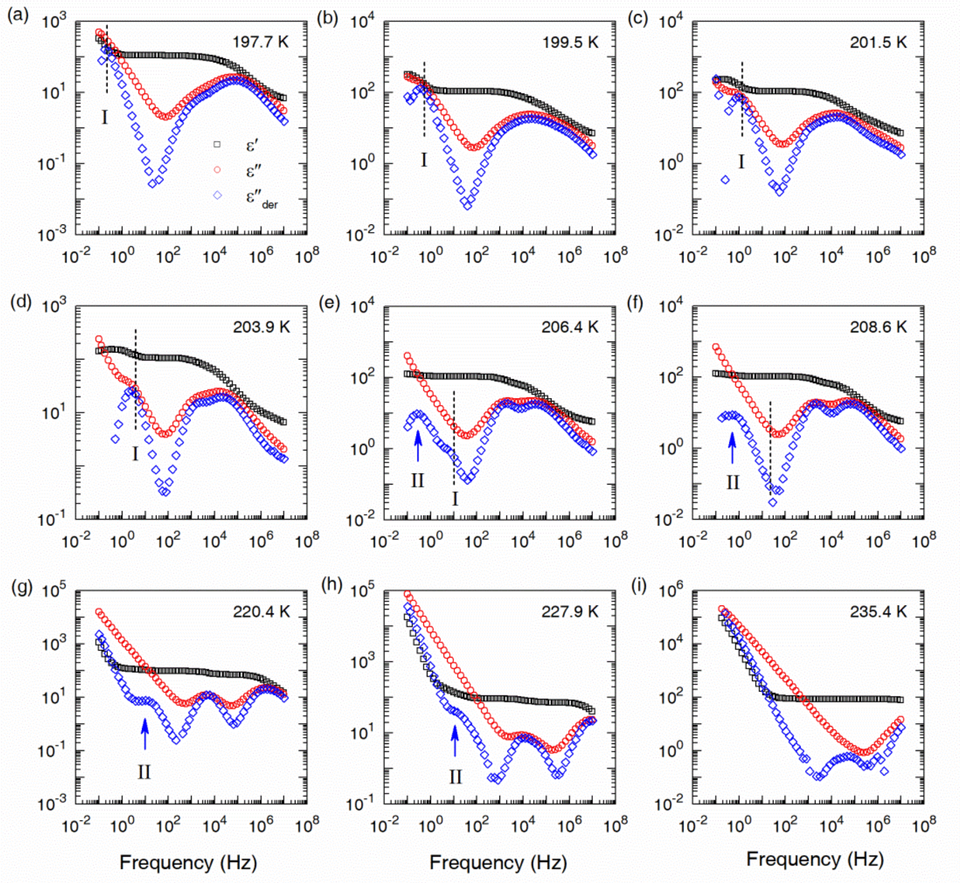

Fig. S3. Frequency dependence of ε' (square), ε'' (circle) and the derivative quantity $\varepsilon''_{der} = -\pi/2 \cdot \mathrm{d}\varepsilon'(\omega)/\mathrm{d}\ln(\omega)$ (diamond) for aqueous glycerol solution with X_w = 0.4 measured during heating the sample from **167 K** up to room temperature at a rate of 0.7 K/min. Sample was previously cooled from room temperature down to **167 K** at a rate of ~10 K/min. For reference, the peak frequency of ε''_{der} for pure glycerol at the corresponding temperature is indicated by a vertical dashed line. It can be concluded that dehydrated glycerol also appears during cold-crystallization of water from the solution, and becomes vanished when cold-crystallization finishes at about 208.6 K (f). Peak II in the derivative quantity ε''_{der} marked by arrow may come from dc conductivity, gas and/or impurities in solution.

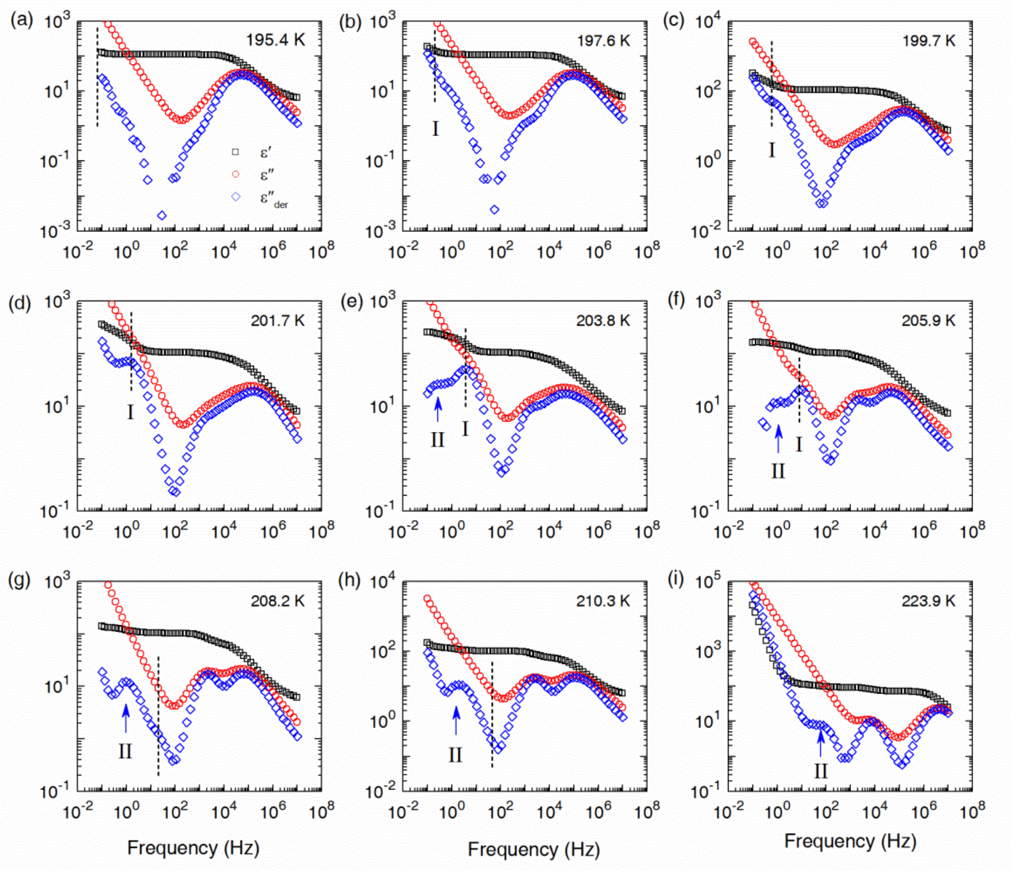

Fig. S4. Frequency dependence of ε'(square), ε''(circle) and the derivative quantity $\varepsilon''_{der} = -\pi/2 \cdot \mathrm{d}\varepsilon'(\omega)/\mathrm{dln}(\omega)$ (diamond) for aqueous glycerol solution with X_{w} = 0.4 measured during heating the sample from ***183 K*** up to room temperature. Sample was previously cooled from room temperature down to ***183 K***. For reference, the peak frequency of ε''_{der} for pure glycerol at the corresponding temperature is indicated by a vertical dashed line. Peak I of ε''_{der} becomes observable when dehydrated glycerol emerges in the process.

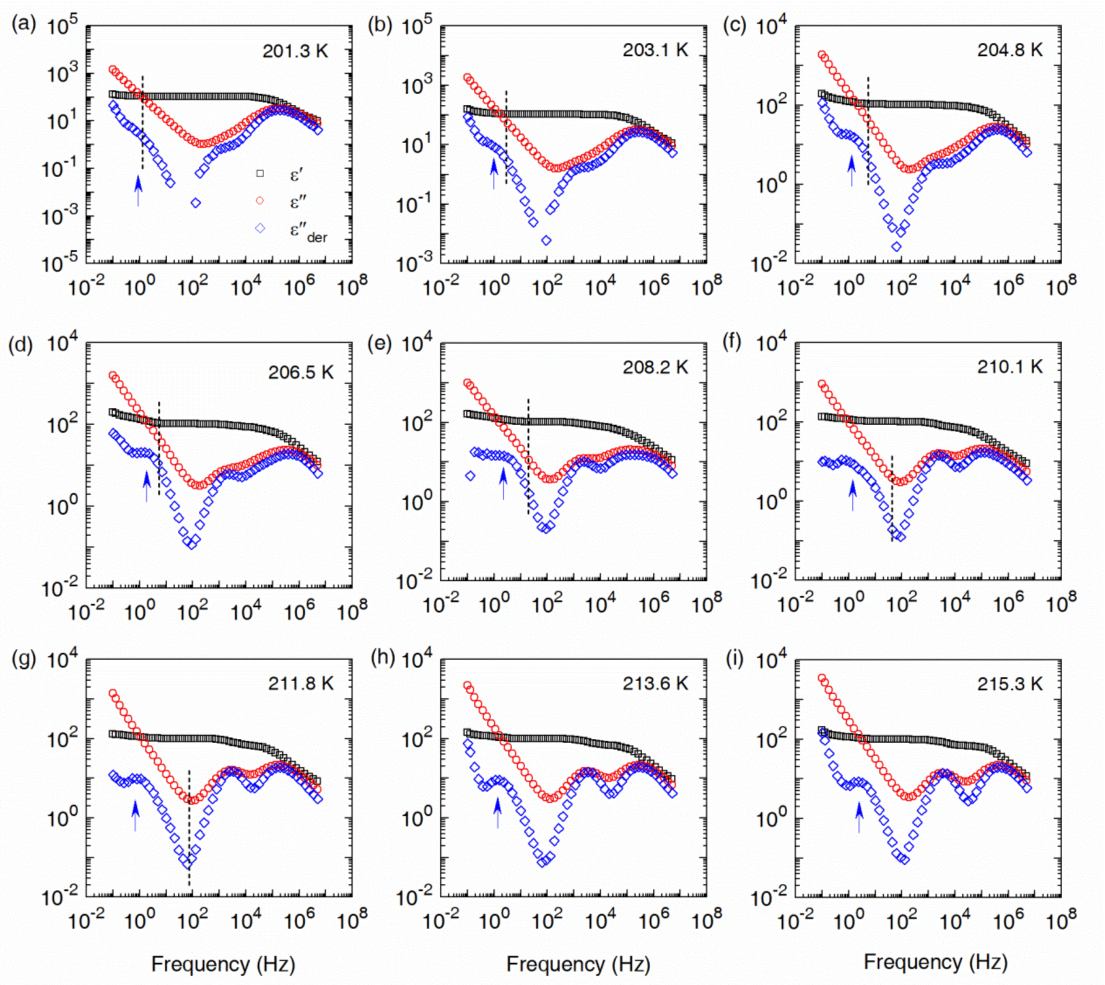

Fig. S5. Frequency dependence of ε'(square), ε''(circle) and the derivative quantity $\varepsilon''_{der} = -\pi/2 \cdot \mathrm{d}\varepsilon'(\omega)/\mathrm{d}\ln(\omega)$ (diamond) for aqueous glycerol solution with X_{w} = 0.4 measured during heating the sample from **188 K** up to room temperature. Sample was previously cooled from room temperature down to **188 K**. For reference, the peak frequency of ε''_{der} for pure glycerol at the corresponding temperature is indicated by a vertical dashed line. In this case the derivative quantity ε''_{der} manifests a peak (arrowed), but it keeps shifting with varied temperature. This low-frequency relaxation process does not come from pure glycerol, but from the dc conductivity instead.

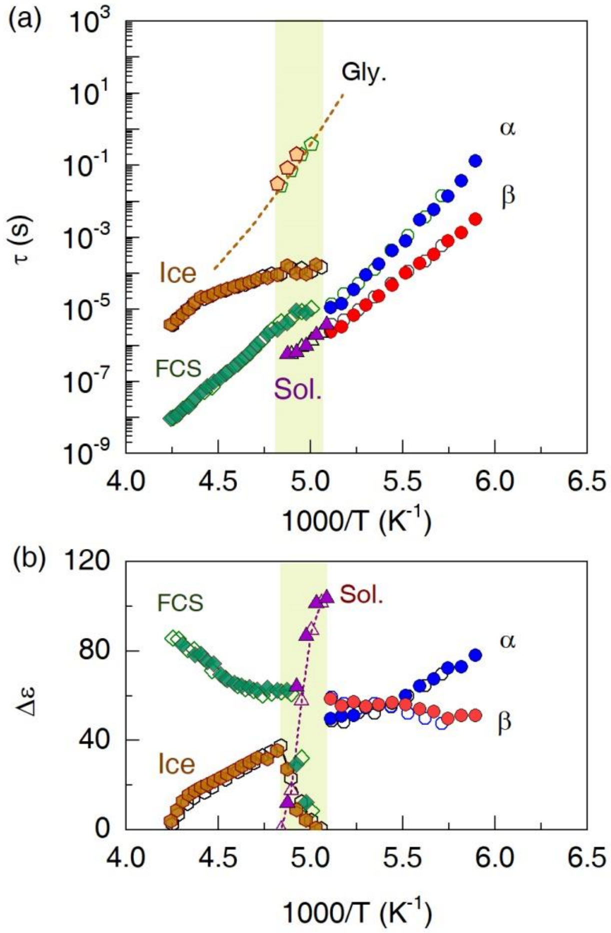

Fig. S6. Inversed temperature dependence of (**a**) relaxation time τ and (**b**) dielectric strength $\Delta\varepsilon$ for α-, β-relaxations (circle), and for those of ice (hexagon), freeze-concentrated solution (FCS, diamond), retrieved solution (Sol., triangle), and a low-frequency relaxation attributable to pure glycerol (Gly., pentagon) for the aqueous glycerol solution with X_{w}= 0.4, measured during heating from T_a= 163 K up to room temperature. Two annealing times, 3 min. (solid symbols) and 300 min. (open symbols), at 163 K were chosen to reveal the effect of holding time on cold-crystallization.

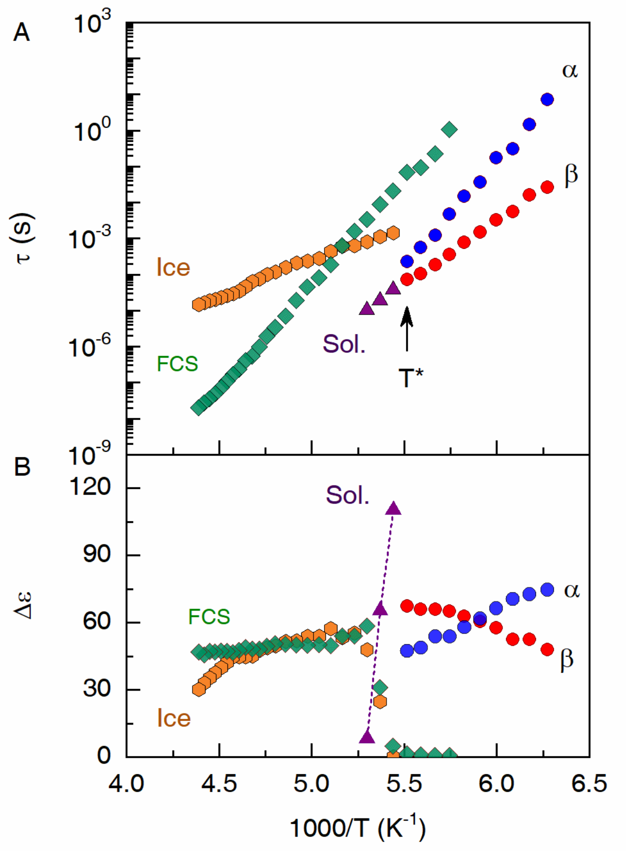

Fig. S7. Cold-crystallization of glycerol solution with $X_\mathrm{w} = 0.44$. Frequency dependence of relaxation time τ (A) and dielectric strength Δε (B) for α-, β-relaxations (circles), and for those of ice (hexagons), freeze-concentrated solution (FCS, diamonds), and retrieved solution (Sol., triangle) measured during heating process from 125 K up to room temperature. The sample was precooled from room temperature to 125 K at ~10K/min. For this aqueous solution, $T_\mathrm{g} = 155$ K, and $T^* = 183.5$ K.

It is not easy to directly determine the amount of ice at temperatures lower thanT^*, because of the closeness of τ_ice to τ_α and even τ_β for intermediate-concentrated glycerol solutions. Fortunately, the relaxation time of freeze-concentrated phase, $\tau_\mathrm{con.}$, is obviously longer than τ_α in the whole measured temperature range. The corresponding $\Delta\varepsilon_\mathrm{con.}$ can help us to estimate $\Delta\varepsilon_\mathrm{ice}$ at temperatures lower than T^* based on the ratio of $\Delta\varepsilon_\mathrm{ice}$ to $\Delta\varepsilon_\mathrm{con.}$ shown at temperatures above T^*. The fraction of ice can then be calculated by normalizing $\Delta\varepsilon_\mathrm{ice}$ to its maximum value obtained at about 190 K. About 2 wt. % of the total cold-crystallized ice precipitated at 174 K, which keeps almost unchanged initially but increases sharply just when increasing temperature above T^*. Within the next 5 K (heating rate: 0.7 K/min), non-isothermal cold-crystallization of water completes quickly.